

Microbubble generation for PIV seeding.

J. A. Venning, S. De Vincentis, B. W. Pearce and P. A. Brandner

Australian Maritime College, University of Tasmania, Launceston, Tasmania, 7250, Australia

Abstract

A new device for microbubble generation using small-scale unsteady cavitation of supersaturated water is presented. Cavitation is created in a radial diffuser with a directed outlet for inlet/saturation pressures ranging from 300 to 1000 kPa. The diffuser is formed using an acrylic plate spaced 50 μm above a 0.5 mm diameter outlet. Optical access is provided via the acrylic plate enabling investigation of the basic flow properties of the cavitation and microbubble trajectories using PIV. The size distribution and production rate of the generated microbubbles are measured using diffused-laser shadowgraphy and long-ranging microscopy within the emerging liquid jet. The size distribution of the microbubble population is suitable for PIV, with all bubbles produced being less than 25 μm . Microbubble production rates in excess of 100 million bubbles per second are achievable. The variation of the generated microbubble population for various operating conditions is presented.

Introduction

Microbubbles (bubbles between 1 μm and 1 mm diameter) are used in a range of processes, such as flotation in minerals processing and waste water treatment [6], contrast agents for localised therapeutic delivery in medical applications, for sonication in sonochemistry [8], as nuclei in cavitation research [2] and for diagnostic tracers in liquids where solid particles are undesirable. The latter two applications are of interest for the present work.

Particle Image Velocimetry (PIV) has been used widely in experimental investigations of fluid mechanic problems. The working principle [5] is that tracer particles suspended in the flow are illuminated twice in a short time period (Δt) and captured with a digital camera. A statistical approach of cross-correlating the two images within interrogation windows across the acquisition plane returns an estimate of the average velocity within each region.

The seeding particle of choice in water tunnels has traditionally been solid particles of density close to that of water [11]. These particles are usually 10 to 50 μm in diameter, with good reflectivity due to their large size. In some instances, such as working with large volumes where seeding would be expensive and hard to remove, or cavitation tunnels where remnant particles may act as nucleation points for cavitation events, solid particles are unsuitable to use as tracer particles. Microbubbles, however, present a viable alternative in these situations since they do not require removal. Due to the density differences between air and water, the size of microbubbles is limited due to undesirable buoyancy effects.

A similar device described in [2] was successful at creating bubbles at a wide range of operating conditions, however, coalescence at the nozzle outlet due to low velocities and difficulties of manufacture has led to the design of the current improved device. The simpler manufacturing and high outflow velocities are the major improvements over the previous design.

PIV seeding in a high Reynolds number water tunnel

For the purposes of this paper, an example flow would be the measurement of velocities in a 100 mm window with a camera with resolution 6600×4400 pixels. The magnification factor is 6.6 px/mm. The flow velocity, $U_\infty = 10$ m/s, is representative of the typical scale of experiments in a water tunnel.

A measure of the flow-following characteristics of a microbubble is given by the relaxation time, τ_p , which for low Reynolds number flows (based on the particle's slip velocity), is:

$$\tau_p = d_p^2 \frac{\rho_p}{18\mu_f}, \quad (1)$$

and thus the diameter requirement from the relaxation time is:

$$d_p < \sqrt{\frac{18\tau_p\mu_f}{\rho_p}} \quad (2)$$

Given the typical relaxation time for solid PIV particles is of the order of μs , the diameter requirement for microbubbles to follow the water flow as well as solid particles is that they must be smaller than 100 μm . The fidelity of flow tracers is defined by the Stokes number τ_p/τ_f , which should be less than 0.1[9]. Thus, the smallest resolvable fluid scale, L , is:

$$L = \frac{d_p^2 \rho_p U_\infty}{1.8\mu_f} \quad (3)$$

From [4], the cut-off frequency for accurate flow tracing is:

$$f = 4 \frac{v_f}{\pi} \left(\frac{\varepsilon}{d_p} \right)^2 \quad (4)$$

$$\varepsilon = \left[2.380^n + \left(\frac{0.659}{0.561 - \rho_p/\rho_f} - 1.175 \right)^n \right]^{1/n},$$

where $n = 0.93$. The length-scale and cut-off frequencies from equations 3 and 4 for a range of particle sizes are given in figure 1. For the bubbles of order 10 μm , the flow is resolvable up to frequencies around 70 kHz, with length-scales around 1 μm .

The usual equation for the rise velocity of a buoyant particle (see [10], for example), gives a rise velocity of a 10 μm bubble as 50 $\mu\text{m}/\text{s}$, which is insignificant in the scale of these flows.

For accurate cross-correlations for PIV calculations, the minimum seeding requirement is 4 bubbles per interrogation window. Assuming an interrogation window size of 32 pixels and a laser sheet thickness of 3 mm, the required bubble concentration is 2.5 per mm^3 . Assuming the plume from a bubble generator extends to ~ 50 mm diameter (as observed in similar devices) and homogeneous seeding across the plume, two bubble generators will be necessary each producing 50 million bubbles per second.

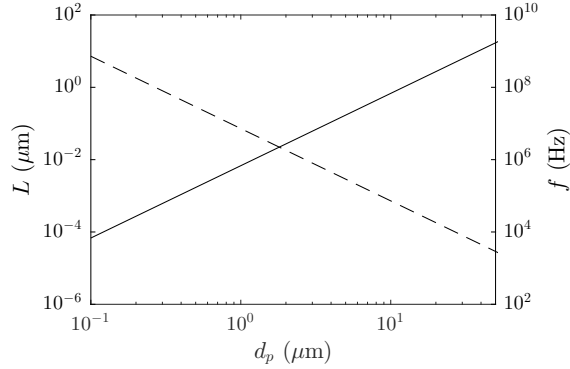


Figure 1: The smallest length-scale (solid), and the cut-off frequency (dashed) for various particle diameters.

Table 1: Non-dimensional parameters.

Parameter	Definition	Range
Re	$\frac{hU_{exit}}{\nu}$	$1.1-1.7 \times 10^3$
σ	$\frac{P_{atm} - P_v}{P_{sat} - P_{atm}}$	0.49–0.11
We	$\frac{h\rho U_{exit}^2}{S}$	380–810

Microbubble generation

A device to generate microbubbles through the cavitation of supersaturated water was designed. The working principle is that a 50 μm shim creates a gap between the saturated-water inlet ($d = 0.5 \text{ mm}$) and a flat surface (figure 2). For the purposes of this study, the material chosen was acrylic to allow visualisation inside the device. Cavitation forms on the sharp-edged exit of the supersaturated water inlet. This causes a contraction in the flow, increasing the flow velocity to in excess of 80 m/s. This high flow velocity results in cavity shedding in the order of 100 kHz. This unsteady shedding results in the formation of microbubbles, which are advected at high speed through the device and out the jet-exit. The non-dimensional parameters of interest in this study are given in table 1.

A double-pulsed Nd:YAG laser was used to illuminate the flow

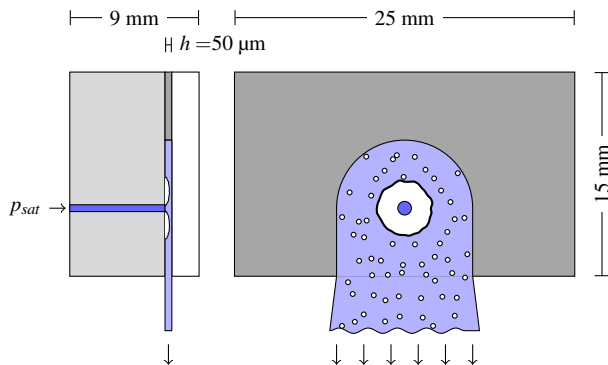


Figure 2: Schematic of the microbubble generation device. The sectional view (left) is through the centre of the saturated water inlet (dark blue), which is a 0.5 mm hole. The cavity is represented by the white area surrounding the water inlet.

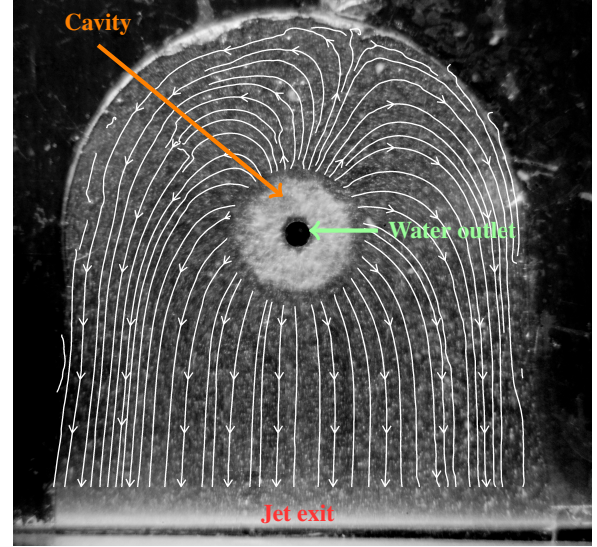


Figure 3: Photograph of the microbubble generating device. The overlaid streamlines are calculated from Bubble Image Velocimetry measurements showing the time-averaged trajectories of bubbles in the device.

inside the device. A multi-pass cross correlation algorithm was used to calculate the bubble velocities inside the device. A set of 1000 image pairs were acquired at a frequency of 1 Hz, such that the images are uncorrelated. Time-averaged streamlines are presented in figure 3.

Compared to previous microbubble generating devices [1], this new design has several advantages. The new device is much simpler to manufacture, consisting only of three faces bolted together, greatly reducing the manufacturing costs. Additionally, previous iterations had strict requirements on the surface finish. The design of this device centred around the principle of advecting the bubbles quickly away from the device. This high advection flow has removed the problem of coalescing bubbles.

The advection flow away from the device is evident in photographs of the micro-bubble plume (figure 4). Here, both the high density of the bubbles and the dispersion of the jet are evident.

The flow-rate through the device for a range of inlet pressures p_{sat} between 300 and 1000 kPa was measured. The discharge coefficient,

$$C_d = U_{exit} \sqrt{\frac{\rho}{2\Delta p}}, \quad (5)$$

is a function of the Reynolds and cavitation numbers as defined in table 1. Figure 5 shows that the discharge coefficient converges to 0.8 for Reynolds numbers beyond 1.5×10^3 , implying a linear increase in exit velocity with the square-root of the pressure difference. The corresponding flow rate range through the device is 10.6–15.5 mL/s.

The cavitation number, σ , is used to describe the extent and nature of the cavitation. A series of photographs of the cavity were acquired for each cavitation number. As the pressure difference increases (σ decreases), the cavity diameter increases (figure 6). It is expected that the number of microbubbles produced will scale with the cavity circumference and local velocity.



Figure 4: Orthogonal photographs of the emerging jet at exit and the dispersing downstream plume of microbubbles.

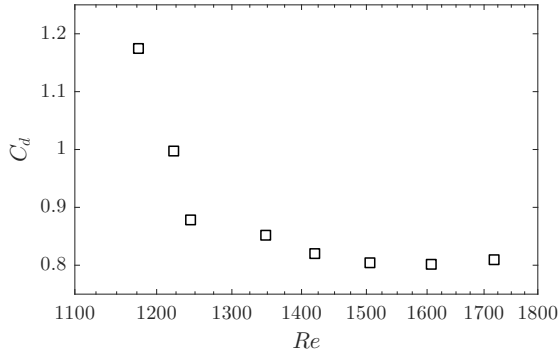


Figure 5: Discharge coefficient through the microbubble generator for various inlet pressures (Reynolds numbers).

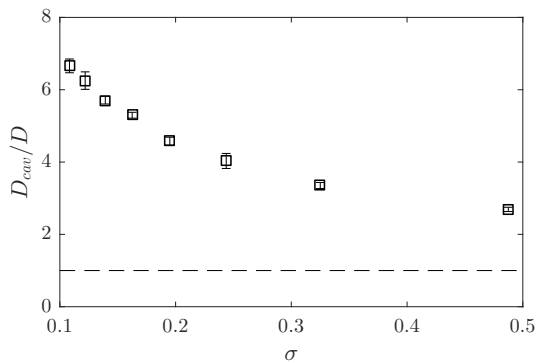


Figure 6: Diameter of the cavity non-dimensionalised by the hole diameter (D) with cavitation number (by variation of the saturation pressure). The standard deviation of the diameter measurement is given with the error bars. Dashed line represents the size of the inlet.

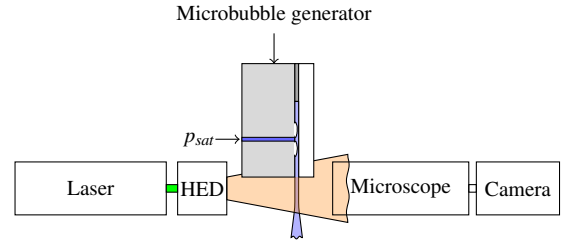


Figure 7: Schematic of the experimental arrangement for shadowgraphy measurements. HED is the High Efficiency Diffuser.

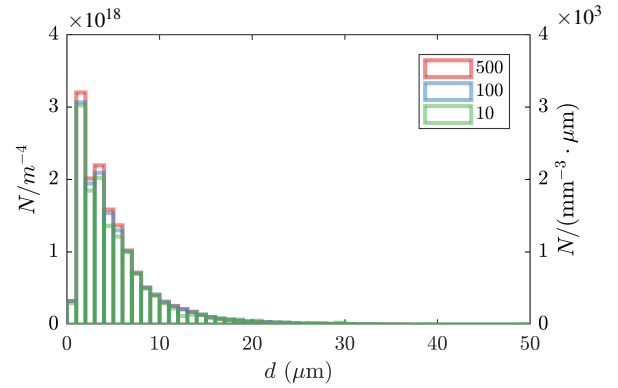


Figure 8: Histograms of the bubble size distribution for $\sigma = 0.13$, as a function of the number of photographs used in the shadowgraphy measurements.

Microbubble population

The generated microbubble populations were measured using shadowgraphy (figure 7), which involved imaging the shadows of bubbles within a measurement volume [7, 3]. The flow at the exit of the device was backlit using a high efficiency diffuser (HED), producing diffuse light with wavelength between 575 and 580 nm. Each pulse was about 20 ns long, sufficiently short to freeze the motion of the microbubbles. The HED was driven by a Litron Nano L PIV Nd:YAG laser.

Shadowgraph images were acquired with a LaVision Imager LX CCD camera, recording 12-bit, 29 megapixel images. A Questar QM-100 long-range microscope was used to achieve a magnification factor of 4.2 px/ μm .

A series of 500 image pairs were acquired for each cavitation number. Pairs were separated by 1 μs to estimate the bubble velocity in the jet. Histograms of the bubble population are given in figure 8, including different numbers of images in the calculation. There are no measurable differences in the distributions above 6 μm . For less than 6 μm the distributions are very similar, even including only 10 images, indicating a very stable population distribution.

The bubble size histograms for the extremes of the pressure range tested (figure 9) reveal that no bubbles larger than 25 μm diameter are produced, which is reasonable given the gap between the two faces is 50 μm . The majority of bubbles are less than 5 μm , and these bubbles will follow the flow across the range of velocities of interest, as discussed above. The distribution is similar for each of the pressures tested, changing only in the rate of bubbles produced.

The total bubble production is given in figure 10. The trend follows that of the cavity diameter as given in figure 6, suggest-

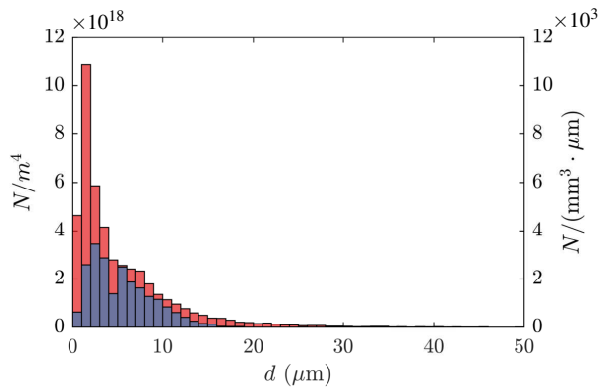


Figure 9: Bubble diameter histogram for $\sigma = 0.49$ (blue) and $\sigma = 0.11$ (red).

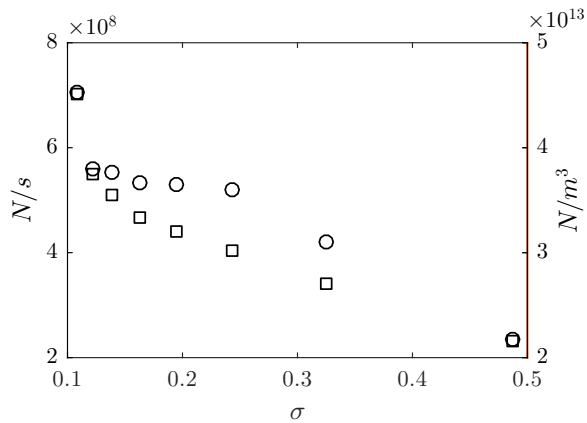


Figure 10: Total count (squares) and microbubble concentration (circles) with cavitation number.

ing that the larger cavity circumferential length is responsible for the increase in bubble production. With this device, up to 700 million bubbles are produced per second, at concentrations up to 45 thousand bubbles per cubic millimetre at outlet. With this production rate, the goal for PIV presented above of 50 million per second is easily achievable. One of the challenges may be in dispersing this flow across the entire PIV plane.

The void fraction at the jet exit is given in figure 11. For low cavitation numbers, this approaches 30%, increasing the likelihood of bubble coalescence. Limits on void fraction to prevent coalescence are yet to be determined but are important to avoid the production of large, undesirable bubbles.

Conclusions

A new device for generating microbubbles using small-scale cavitation in super-saturated water is presented. The device was characterised for various cavitation and Reynolds numbers. Shadowgraphy measurements were used to estimate the production frequency and size distribution of the generated microbubble population. The microbubbles are shown to be of a suitable size for PIV measurements, all less than 25 μm . The production rate of hundreds of millions of bubbles per second is sufficient for seeding a 100 mm PIV acquisition plane.

Acknowledgements

The authors acknowledge the contributions of Steven Kent and Robert Wrigley in manufacturing the microbubble generator. Support from DSTG is also appreciated.

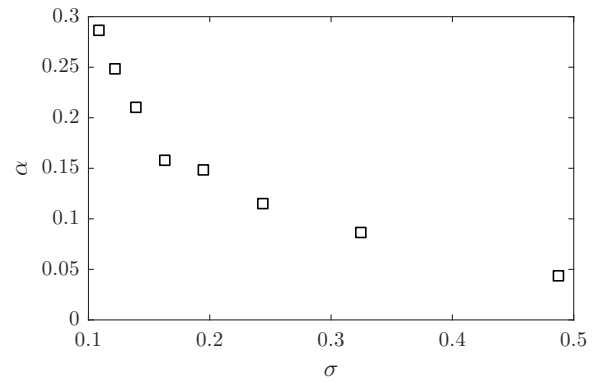


Figure 11: Void fraction at the jet exit with cavitation number.

References

- [1] Brandner, P. A., Graaf, K. L. D., Pearce, B. W. and Burgess, J. S., Microbubble Generation in a Confined Radial Jet, in *19th Australasian Fluid Mechanics Conference, Melbourne*, 2014.
- [2] Brandner, P. A., Pearce, G. W. B., Goldsworthy, L. and Walker, G. J., An Experimental Investigation of Microbubble Generation in a Confined Turbulent Jet, in *17th Australasian Fluid Mechanics Conference*, 2010.
- [3] Giosio, D., Pearce, B. W. and Brandner, P. A., Influence of Pressure on Microbubble Production Rate in a Confined Turbulent Jet, in *20th Australasian Fluid Mechanics Conference*, 2016.
- [4] Mei, R., Velocity fidelity of flow tracer particles, *Experiments in Fluids*, **22**, 1996, 1–13.
- [5] Raffel, M., Willert, C. E., Wereley, S. T., Kompenhans, J. and Springer, J., *Particle Image Velocimetry - A Practical Guide*, Springer, 2013.
- [6] Rodrigues, R. T. and Rubio, J., New basis for measuring the size distribution of bubbles, *Minerals Engineering*, **16**, 2003, 757–765.
- [7] Russell, P. S., Giosio, D. R., Venning, J. A., Pearce, B. W. and Brandner, P. A., Microbubble Generation from Condensation and Turbulent Breakup of Sheet Cavitation, in *31st Symposium on Naval Hydrodynamics*, 2016.
- [8] Suslick, K. S. and Flannigan, D. J., Inside a Collapsing Bubble : Sonoluminescence and the Conditions During Cavitation, *Annual Review of Physical Chemistry*, **59**, 2008, 659–683.
- [9] Tropea, C., Yarin, A. L. and Foss, J. F., *Springer Handbook of Experimental Fluid Mechanics*, Springer Science & Business Media, 2007.
- [10] van Overbrüggen, T., Schröder, F., Klaas, M. and Schröder, W., A particle-image velocimetry tracer generating technique for liquid flows, *Measurement Science and Technology*, **25**.
- [11] Venning, J., Lo Jacono, D., Burton, D., Thompson, M. and Sheridan, J., The effect of aspect ratio on the wake of the Ahmed body, *Experiments in Fluids*, **56**, 2015, 126.